Biocatalysis and Agricultural Biotechnology 18 (2019) 101075

Contents lists available at ScienceDirect

Biocatalysis and Agricultural Biotechnology

journal homepage: www.elsevier.com/locate/bab

Phyto-synthesis of silver nanoparticles and its bioactivity response towards nosocomial bacterial pathogens

Khamis Al-Dhafri*, Chai Lay Ching

Microbial Biotechnology Laboratory, Department of Genetics and Microbiology, Faculty of Science, University of Malaya, Kuala Lumpur, 50603, Malaysia

ARTICLE INFO

Keywords:
Silver nanoparticles
Protein
Antibacterial
Biomolecules
Cytotoxicity

ABSTRACT

The emergence of antimicrobial resistance is a major concern for public health. In this study, naturally occurring plant *Juniperus chinensis* leaf (JCL) extract used for the synthesis of silver nanoparticles (AgNPs) with enhanced antimicrobial effect. The unresolved phyto-protein synthesis mechanism of AgNPs was preliminarily detected by LCMS/MS analysis. The study revealed that the non-specific lipid transfer protein (LTP) and Cytochrome *b*559 subunit beta were detected from JCL could be responsible for AgNPs synthesis. The JCL protein readily reacts with the $AgNO_3$ to form highly stable AgNPs. The synthesized AgNPs were characterized by UV-Vis spectroscopy, FTIR, XRD and HRTEM analysis. Further, the antibacterial mechanism of AgNPs was analyzed by electron microscopy and CLSM analysis. Moreover, the AgNPs showed the potent anticancer effect on the human adenocarcinoma gastric (AGS) cell lines. The current study will provide additional support to overcome the limitations of large-scale NPs synthesis which could be used to alternate source for conventional antibiotics.

1. Introduction

Silver nanoparticles are one of the superior nanomaterials that directly or indirectly involve in our daily life (Singh and Sahareen, 2017). In last two decades, nano-Ag materials has been categorizing the centralized area of modern researchers especially in biomedical field due to their unprecedented health benefits including superior antimicrobial efficacy (Iniyan et al., 2017; Judith Vijaya et al., 2017), wound healing (Wang et al., 2018) and anticancer (Gopinath et al., 2016a,b) activity. The variety of physico-chemical procedures been employed to synthesize the size and shape tailored silver nanoparticles that remain the primary concern of environmental and cell toxicity due to the utilization of hazardous materials (Amooaghaie et al., 2015). To overcome these issues biological materials such as plants, bacteria, yeast, virus, proteins, and peptides have been extensively used for metal nanoparticles (MNPs) synthesis using green chemistry procedures where the materials itself serve as reducing/stabilizing agents (Ahmad et al., 2013; Gopinath et al., 2012; Gopinath et al., 2016a,b; Gopinath et al., 2013; Gopinath et al., 2017; Gopinath and Velusamy, 2013; Hulkoti and Taranath, 2014). Amongst the biological entities, phyto-based materials are being recognized massively due to its ease of availability and economical reliability (MubarakAli et al., 2011).

Phyto-mediated synthesis is one of the most prevalent methods of green synthesis due to cost-effective, abundantly renewable and eco-friendly materials (Jha et al., 2009; MubarakAli et al., 2011). However, the mechanism of MNPs synthesis was mostly unknown. Few researchers partly evidenced the proteins or peptides present in the biological materials involved in the synthesis and stabilization of the MNPs (Gopinath et al., 2015; Naik et al., 2002). Among the various metal NPs, AgNPs have attracted considerable attention due to its unique biological and physicochemical properties. The recent study reported that the synthesis of highly-stable Ag based materials using bacterial protein through photo-biosynthesis required light irradiation and HCL treatment along with the $AgNO_3$ (Araújo et al., 2017). From ancient to till date Ag and its nano-formulation are well known for its antimicrobial profile since then the continuous effort has been applied to achieve superior antimicrobial formulation for the ever-growing multidrug-resistant bacterial pathogens (Davoodbasha et al., 2016; Hu et al., 2009). AgNPs expressed the unique functional, mechanical and biological properties based on their morphological structure, size and had larger surface area compared to the bulk silver. These remarkable properties offered nanosilver as the superior material for many biomedical and nanotechnological applications (Ahmed et al., 2016).

In this study, we synthesized AgNPs using the *J. chinensis* extract and evidenced that the plant protein-mediated synthesis and stabilization. *J. chinensis* ornamental plant is known as Chinese juniper and widely spread in the East Asian region. It composed of three major chemical compounds such as flavones, lignins, and terpenes (Lee et al.,

* Corresponding author.
E-mail address: aldhafri2013@siswa.um.edu.my (K. Al-Dhafri).

https://doi.org/10.1016/j.bcab.2019.101075
Received 8 December 2018; Received in revised form 26 February 2019; Accepted 3 March 2019
Available online 06 March 2019
1878-8181/

1995). *J. chinensis* had been widely used for a variety of medicinal purposes including in folk medicines for centuries ago (Orhan et al., 2011). To the best of our knowledge, this is the first report of antibacterial AgNPs synthesis using *J. chinensis* plant protein extract.

2. Materials and methods

2.1. Plant materials and compounds extraction

The plant leaf materials of *Juniperus chinensis* were obtained from the University of Malaya campus, Kuala Lumpur, Malaysia and surface cleaned with sterile water. After that, leaves were dried under direct sunlight for 48 h and ground to make a fine powder using a stainless blender. The powder was exposed to 500 mL of 80% methanol (MeOH) for 3 days at 4 °C. Then the extract was subsequently filtered and concentrated using a vacuum rotary evaporator at 40 °C giving semi-solid extracts affording about 15% yield (w/w), and freeze-dryer was used to powder the extraction after evaporation of methanol.

2.2. Microorganisms and cell line maintenance

The tested bacterial pathogens *Escherichia coli, Staphylococcus aureus, Pseudomonas aeruginosa,* and *Bacillus subtilis* were obtained from the laboratory collection of the Department of Microbiology and Genetics, University Malaya, Malaysia. The strains were cultured and maintained in nutrient agar (NA) media. Gastric adenocarcinoma AGS cells (#43504) were obtained from the American Type Culture Collection, and cultured using Rosewell Park Memorial Institute 1640 (RPM1640) medium (Biowest) supplemented with 10% fetal bovine serum.

2.3. Phyto molecules synthesis of AgNPs

The above prepared plant extract 100 mg W/V was exposed to the final concentration of 1 mM $AgNO_3$. Then the reaction solution was boiled at 100 °C for 60 min under the dark condition. The nanoparticles growth and formation were observed by the color change of the reaction solution as well as recording the UV–vis spectrum (Zayed et al., 2019).

2.4. Phyto-protein extraction

The sample was prepared and followed by (Taha et al., 2014) to identify active biomolecules which actively involved in the synthesis of AgNPs. The mass spectrometer (AB Sciex TripleTOF 4600) instrumentation set up, solvent gradient flow rate, for sample analysis, were followed by (Nordin et al., 2014). The turbo ion source settings were as follows: capillary voltage, 500 V; dry gas flow rate (N2), 9 L/min; nebulizer pressure, 35 psi; and capillary temperature, 500 °C. A full scan of the mass spectra recorded from m/z 50 to m/z 1000. The observed MS/MS spectra results were analyzed using Analyst software (version 1.5.1). The samples examined by LC-MS/MS analysis and the raw data saved and analyzed with Proteome Discoverer 1.3.0.339 software suite (Thermo Scientific). The LCMS data result helps to detect the molecular weight of peptides resulting in naming the isolated compounds.

2.5. Characterization of synthesized nanoparticles

UV–vis absorption spectra of the NPs synthesis reaction mixture and the plant protein compounds were measured by UV–vis spectrophotometer at the wavelength of 200–700 nm at a resolution of 1 nm. The synthesized nanosilver particles size and structural morphology were analyzed using High-Resolution Transmission Electron Spectroscopy (HRTEM) on a JEOL, JEM-2100 F. The crystalline nature of the particles was recorded by X-ray diffractometer instrument on Bruker, AXS with Cu-Kα radiation (λ = 1.5418 Å) at the scan speed of 2°/min. The chemical composition present in the nanoparticles surface was analyzed using energy dispersive X-ray spectroscopy (EDAX) result in STEM mode.

2.6. Antibacterial efficacy of AgNPs

The antibacterial effect of AgNPs was determined against both Gram-positive and negative nosocomial bacterial pathogens such as *B. subtilis*, *E. coli, S. aureus,* and *P. aeruginosa* by following (Gopinath et al., 2016, 2019). Briefly, the bacterial inhibitory assay was performed using Muller Hinton broth (MHB). The freshly grown bacterial culture was diluted to achieve the concentration of 10^8 CFU/mL, measured using the OD at 600 nm. MHB was dispersed into the 96 wells with the exposure of AgNPs. The plate wells were serially diluted by adjusting the nanoparticles concentrations to reach at 1.25–50 μg/mL. The wells containing the MHB alone and bacterial suspension were considered as a negative and positive control respectively. The AgNPs concentration which inhibits the bacterial growth approximately 50% was considered as MIC_{50}. The bacterial suspension displaying no visible growth were cultured on NA plates and incubated at 37 °C for 24 h. After that, the plates were observed no significant growth was considered as minimum bactericidal concentration (MBC_{99}).

2.7. Bacterial membrane integrity of AgNPs

The bacterial structural and morphological changes triggered by AgNPs were analyzed using electron microscopy techniques. One Gram-positive strain *S. aureus* and a Gram-negative strain *P. aeruginosa* was studied for the morphological analysis upon AgNPs treatment. The NPs exposed bacterial sample preparation was followed by (Saravanan et al., 2018). The samples were observed under FESEM (JEOL JSM-7001 F, Germany) to determine the structural changes caused by the AgNPs treatment.

2.8. Bacterial (live/dead) viability assay

Phyto-AgNPs induced bacterial cell damage was analyzed under a confocal laser scanning microscope (SR-CLSM; LSM880 with Airyscan, ZEISS, Oberkochen, Germany). The bacterial cells (10^5 CFU mL^{-1}) before and after exposure with their MIC concentration for AgNPs were incubated for 1 h and 2 h at 37 °C under shaker incubator. Then the cells were washed twice with PBS and stained with the (LIVE/DEAD™ BacLight™) kit containing SYTO 9 and propidium iodide Bacterial Viability Kit for microscopy L7007, Invitrogen Detection Technologies, ThermoFisher scientific, Seoul, South Korea). The instruction manual was followed to stain the bacterial cells. The fluorescence excitation and emission wavelength were followed by the earlier report (Saravanakumar et al., 2018).

2.9. In vitro toxicity of AgNPs on AGS cells

The human gastric AGS cells were used as a model organism to determine the toxicity of AgNPs. The MTT colorimetric assay was followed by the earlier published protocol (El-Naggar et al., 2017) with a slight alteration. The generation of formazan is directly related to the number of live cells and in reverse proportionate to the cell toxicity. The cultured cells were removed using trypsin–ethylenediamine tetraacetic acid (EDTA) and seeded approximately 10,000 cells/well on to the microtitre plate and incubated for 24 h at 37 °C, 5% CO_2, 95% air and 100% relative humidity. The cells were exposed to increasing AgNPs dosage for 24 h. The AgNPs dosage was serially diluted at (3.125, 6.52, 12.5, 25, 50, 100 μg/mL) were exposed to 100 μL cell suspension. The wells were incubated for 24 h at the above condition. The sample tested concentrations (3.125, 6.52, 12.5, 25, 50, 100 μM) of 5-fluorouracil (5-FU) were served as a standard. The experiment was

repeated thrice to ensure data accuracy. Meanwhile, 20 µL of MTT was added to PBS (5 mg/mL) in the wells and incubated at 37 °C for 4 h for the reduction of MTT. Then 100 µL of DMSO was used to solubilize the formazan, and the plates were read at an absorbance of 570 nm using a plate reader, and the cytotoxicity was analyzed (El-Naggar et al., 2017).

2.10. Apoptosis effect of AgNPs

The apoptotic toxicity level to the AGS cells was determined by the Tali apoptosis kit composed of fluorescent dyes Annexin V – AlexaFlour 488 (Green) and propidium iodide (red). Briefly, the cells were exposed to the above, increasing concentration of AgNPs for 24 h. Then the experimental procedure was shadowed by (Rizwan et al., 2018) where the Tali apoptosis kit instruction manual was followed. Finally, the stained cells loaded slide was inserted into the Tali image-based cytometer slide chamber via capillary force, and the apoptotic toxicity was recorded.

2.11. Statistical analysis

The experimental data were expressed in the mean ± standard deviation of triplicates, and the statistical significance was determined with oneway ANOVA, P-value < 0.05 were accepted as statistical significance using Sigmaplot 12 software.

3. Results and discussions

3.1. Phyto-synthesis of AgNPs

Phyto-synthesis of MNPs eliminates the toxicity associated problems in the traditional physio-chemical systems with an advantage of economically low cost, renewable and eco-friendly approach. Here AgNPs phytosynthesis was carried out by using the aqueous antimicrobial *J. chinensis* extract with aqueous $AgNO_3$. The plant protein has reduced the bulk silver ions into nanosized AgNPs was confirmed by the color change of reaction mixture from light yellow to brown designating the formation of silver nanoparticles (Gopinath et al., 2013). The observed color is due to the excitation of surface Plasmon vibrations of silver nanoparticles (Gopinath et al., 2016a,b). Conversely, no color change was observed in aqueous $AgNO_3$ alone and the plant extract under the same conditions.

3.2. LCMS/MS analysis

The LCMS resultant peak was picked and compared with the Mascot SwissProt database. The observed spectrum in (Fig. 1) all the 10 mass protein coverage were selected and analyzed through the SwissProt database. There were only 4 matches were found with 329.0, 377.0, 377.0 and 505.2 with sequence similarity. However, the high similarity was observed for (NLTP6_AMBAR) the non-specific lipid transfer protein (LTP) and (PSBF_TETOB) Cytochrome *b*559 subunit beta present in the plant extract.

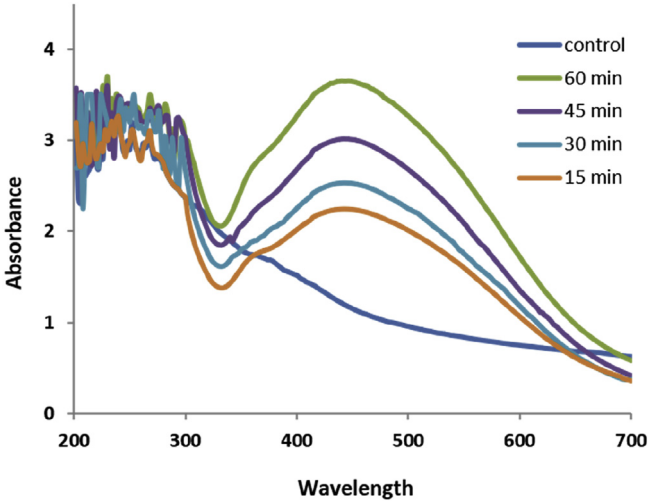

Fig. 2. The UV-visible spectrum of plant extract and its synthesized AgNPs at the increasing time period of 0–60 min (a).

3.3. UV-visible spectrum study

UV-Vis spectrum analysis was generally used to study the metal nanoparticles formation in the aqueous reaction medium. The reaction mixture was scanned at 200–700 nm, at the time interval of 0–60 min. The surface plasmon resonance (SPR) characteristics of AgNPs synthesized by phyto-protein indicate the peak at 455 nm (Fig. 2), was correlated well with the earlier report of AgNPs biosynthesis using phyto-extracts (Ashraf et al., 2016). The increasing peak intensities of observed SPR peak indicated the nucleation as well as the generation of nanosilver particles in the aqueous medium (Ahmad et al., 2017).

3.4. Crystalline study of synthesized nanoparticles

The XRD spectrum pattern of synthesized nanoparticles (Fig. 3), showed the peaks were observed at 2θ of 38.6°, 46.3°, 64.8°, and 77.1° can be indexed to (111), (200), (220) and (311) reflections respectively, which is the characteristics of the of AgNPs. The results indicate that the phyto-synthesized AgNPs are highly crystalline, and the observed peaks are in good agreement with the earlier reports of green synthesized AgNPs. Also, the observed sharp peaks indirectly propose the smaller size of the synthesized AgNPs.

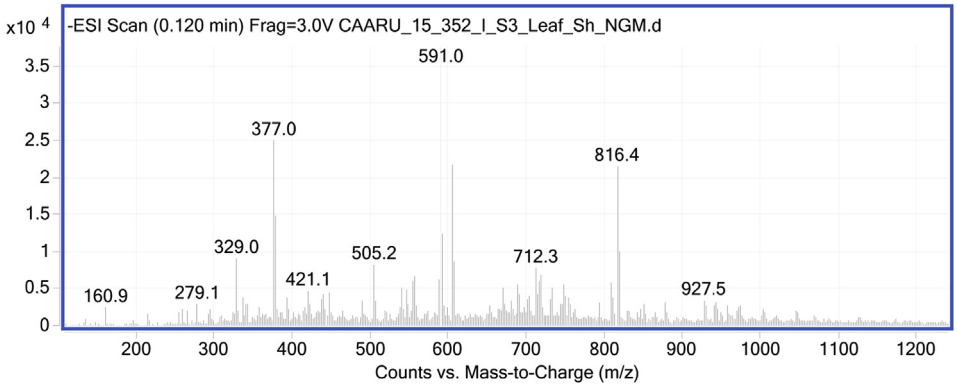

Fig. 1. The LCMS spectrum of *J. chinensis* plant extract shown 10 intense peaks were only 4 were matched with NCBI protein database.

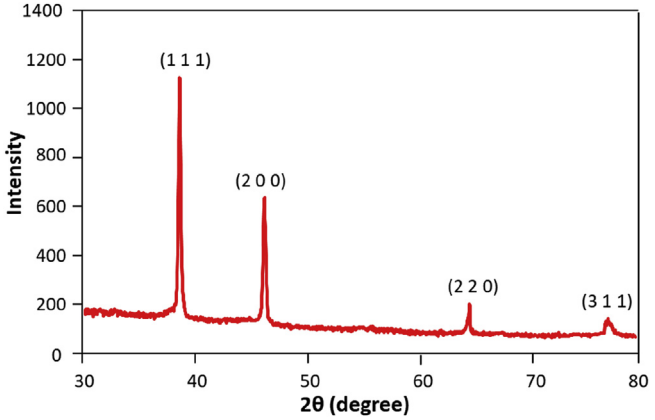

Fig. 3. XRD spectrum of green AgNPs (a) indicated the particles were pure and highly crystalline. (For interpretation of the references to color in this figure legend, the reader is referred to the Web version of this article.)

3.5. AgNPs morphological analysis

The HRTEM micrograph images (Fig. 4a), showed the phyto-synthesized AgNPs were differentially shaped, and the average sizes were found to be in the range of 18–25 nm. However, the majority of the particles were not aggregated, and most of the AgNPs appeared to be capped with irregular-shaped substances which are believed to be the phyto-substances. Further, the elemental spectrum analysis results showed the strong signals were observed at Ag confirming the nanoparticles formation and, the observed Al peak was due to the aluminium foil which was used to load the AgNPs for analysis (Fig. 4b).

Table 1
Antibacterial effect of phyto-silver nanoparticles against the Gram-positive and negative bacterial pathogens.

S.No	Test bacterial pathogens	AgNPs concentration (μg/mL)	
		MIC	MBC
1.	*E. coli*	15	18
2.	*P. aeruginosa*	14	18
3.	*S. aureus*	18	21
4.	*B. subtilis*	17	20

3.6. MIC and MBC for AgNPs

To assess the bacterial inhibitory effect of AgNPs, the cell suspensions were serially diluted and monitored after 24 h of incubation. Then the plates were accessed the inhibitory effect of bacterial growth, and the data were compared with the blank (bacterial suspension) and the (MHB). The observed growth inhibition of tested bacterial strains is shown in (Table 1). The effect of AgNPs significantly inhibited all the measured bacterial growth.

Moreover, green synthesized AgNPs displayed a better antibacterial efficacy on bacterial strains than conventionally synthesized particles (Suresh et al., 2010). Firstly, we also confirmed the antibacterial effect of plant extract concentration applied for AgNPs synthesis which did not display a considerable inhibitory effect against the bacterial

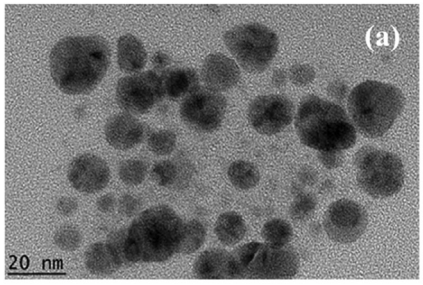

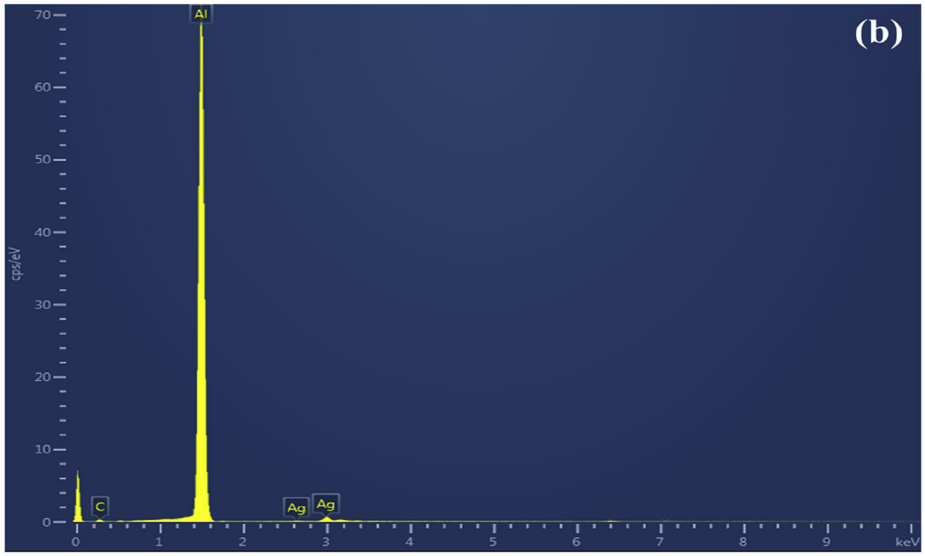

Fig. 4. The HRTEM image of plant-mediated AgNPs showed the structural morphology and size of the particles (a), energy dispersive X-ray (EDS) spectra observed silver signal indicated the synthesized AgNPs was highly pure and confirmed the NPs formation (b).

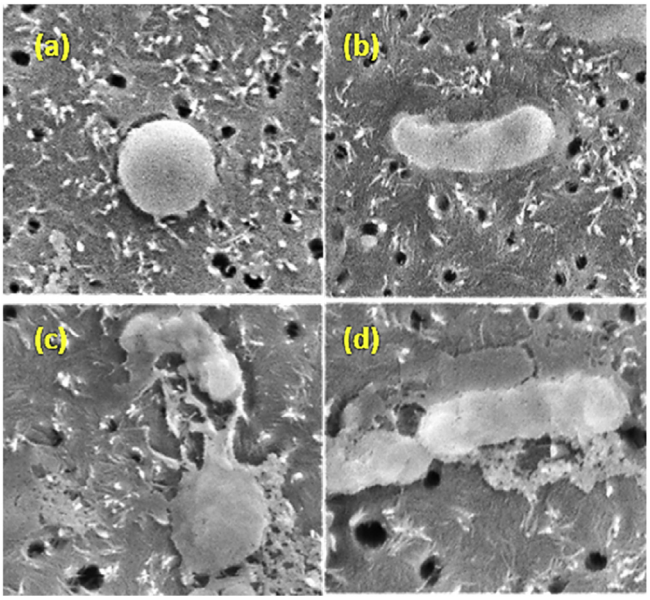

Fig. 5. Electron microscopic images of AgNPs exposed and unexposed bacterial pathogens. The control cells found to be healthy with the clear cell membrane (a,b). The cell membrane penetration was noticed upon the nano exposure induced the excretion of cellular metabolites caused cell death (c, d).

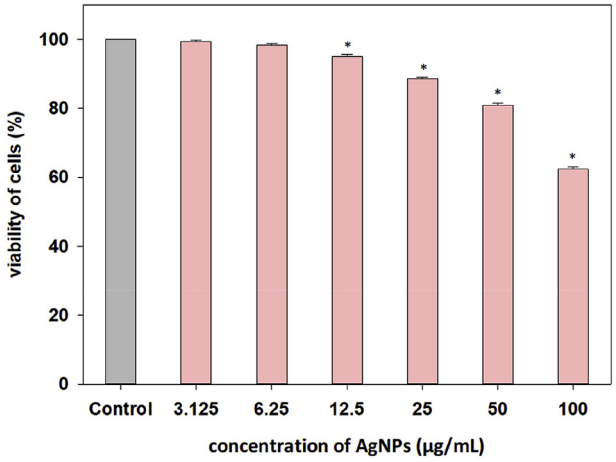

Fig. 7. Biocompatibility assay of AgNPs on AGS cells. (A) Assessment of cellular toxicity on the AGS cells exposed to 3.125–100 µg/mL AgNPs for 24 h * indicates significant reduction of ($p < 0.01$) compared with control. The result showed the significant cytotoxicity at 50 µg/mL of AgNPs.

pathogens. AgNPs possess noticeable microbicidal effects due to its large surface area, which offers higher interaction with bacterial pathogens and adhered to the cell membrane through membrane penetration. AgNPs are known to interact with the cell membrane proteins containing phosphorus, sulfur constituents in the cell (Rasheed et al., 2017). Further, it is noteworthy to mention that the NPs showed the higher inhibitory effect mainly on the Gram-negative bacteria of *E. coli* and *P. aeruginosa* at 15 and 14 µg/mL where it was found to be significantly low at the same concentration against the Gram-positive *S. aureus* and *B. cereus* unless increased to 18 and 17 µg/mL. As expected, the positive and negative controls did not expose any inhibitory effect. Also for the first time, we primarily identified the AgNPs synthesis mechanism to enhance the large-scale production of antimicrobial nanosilver materials.

3.7. Membrane integrity of green nanoparticles

Electron microscopic images recorded the bacterial membrane damage caused by AgNPs exposure. The tested bacterial strains control of *S. aureus* and *P. aeruginosa* without nanoparticles exposure was observed (Fig. 5a and b) with the intact membrane indicates the cells were healthy and viable. Further, the AgNPs treated bacterial cells were observed with dented plasma membrane which subsequently leads to

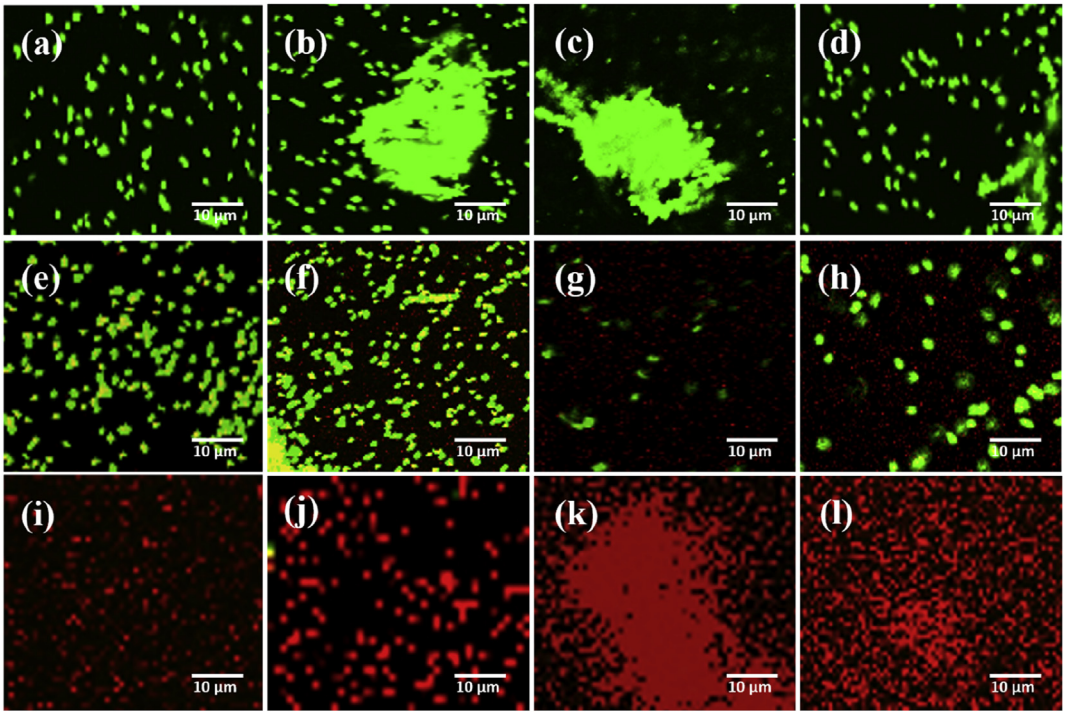

Fig. 6. (A–d) CLSM images of selected nosocomial pathogens without AgNPs treatment. The cells subjected with AgNPs after 1 h fluoresced orange, green dots (e–h) and after 2 h of treatment, all the cells were fluoresced red color. (For interpretation of the references to color in this figure legend, the reader is referred to the Web version of this article.)

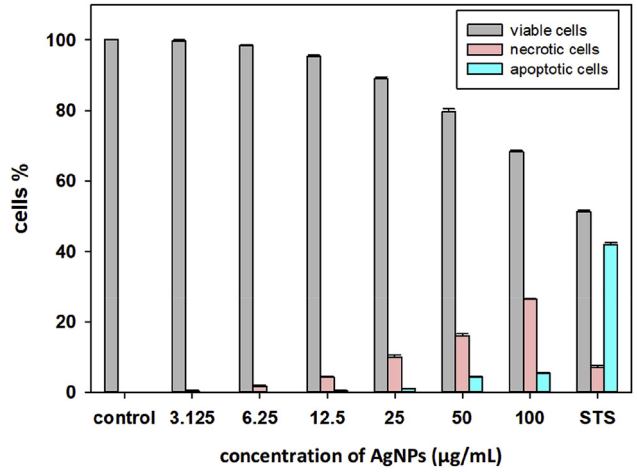

Fig. 8. Apoptotic toxicity of plant-mediated synthesis of AgNPs. The significant percentage of apoptosis toxicity was observed at 50 µg/mL, whereas the apoptotic/necrotic toxicity was increased at the higher nanoparticles dosage.

cell death (Fig. 5c and d). The observed result was correlated well with the earlier reports of bacterial membrane integrity (Saravanan et al., 2018). The nanoparticles exposed bacterial cells observed as hollow, distorted and clutched, representing a severe membrane impairment followed by the release of cellular components (Ahmad et al., 2017).

3.8. Viability assay

The bacterial membrane damage and cell death caused by the action of AgNPs was also confirmed by Live/Dead viability assay. The CLSM image of untreated bacterial pathogens was shown green fluorescent color which indicates high viability of 99% (Fig. 6a–d). The nanoparticles exposed bacterial cells after 60 min was observed the orange, green color spots due to the nucleic acid stain PI bind to the damaged bacterial membrane (Fig. 6e–h) which leads to the excretion of cellular components (Maruthupandy et al., 2018). The more extended incubation period (120 min) of bacteria-AgNPs which were eventually increased the cell death was observed maximum percentage of red spots (Fig. 6i–l) (Xie et al., 2017).

3.9. MTT assay

To investigate the MTT cytotoxicity effect of plant-mediated AgNPs depending on the metabolically viable cell that reduces MTT to purple color formazan. AGS cells were exposed to the increased dosage of AgNPs, and then the plates were kept in the CO_2 incubator. The cells were monitored at 24 h of post-NPs treatment with 3.125–100 µg/mL AgNPs, expressed that the particles were not cytotoxic up to 25 µg/mL. However, the increased dosage of AgNPs at 50≤ µg/mL (Fig. 7) represents the significant reduction of viability at 23% reflects the dose-dependent toxicity (Rizwan et al., 2018). In particular, the observed data suggesting the green synthesized AgNPs have greater biocompatibility where it completely inhibits the bacterial pathogens even its minimal dosage.

3.10. Apoptotic toxicity assessment of AgNPs

The apoptotic toxicity level upon the AgNPs exposure to AGS cells was examined after 24 h, where the cells were mixed with the green and red fluorescent stains Annexin V and PI (Fig. 8). The resulting data indicated that the AgNPs did not show any significant level of apoptotic toxicity to the AGS cells at ≥25 µg/mL. Nonetheless, the AgNPs dosage was increased from 50 to 100 µg/mL were detected the significant level of toxicity. Our result also supported by the above MTT dose-dependent cytotoxicity of AgNPs. It was reported that the AgNPs treatment generated the mitochondrial damage and excretion of cytochrome *c* to the cells (Ma et al., 2011). The discharge of mitochondrial cytochrome *c* into the cytoplasm induces the cell apoptosis and is reflected the apoptotic induction to the cells (Rajabnia and Meshkini, 2018). Together with the outcomes, the above cell cytotoxicity was concurrent with the apoptotic toxicity.

4. Conclusion

AgNPs was successfully synthesized using the plant antimicrobial compound from *Juniperus chinensis*. Characterization of the phyto-synthesized AgNPs was analyzed by UV–Vis, TEM, EDX and XRD spectrum confirmed the crystalline nature of AgNPs with the average size of 24 nm. In the mechanistic view, we primarily reasoned the protein molecules present in the extract which generated the synthesis and stability of AgNPs. Firstly, we detected the significant synergistic effect of synthesized AgNPs against the tested bacterial pathogens. We conclude the bacterial membrane damage was induced the leakage of cellular metabolites could also be reasoned for the bacterial toxicity. Convincingly the synthesized AgNPs express the lesser cytotoxicity to the human AGS cell lines proves that the NPs are highly biocompatible. Together the resulting data we have concluded the AgNPs could be effectively used for the replacement of conventional antibiotics.

Acknowledgements

The author greatly acknowledge Department of Genetics and Microbiology, Faculty of Science, University of Malaya and Biology Department, College of Science, Sultan Qaboos University for providing support to carry out the study.

References

Ahmad, A., Wei, Y., Syed, F., Tahir, K., Rehman, A.U., Khan, A., Ullah, S., Yuan, Q., 2017. The effects of bacteria-nanoparticles interface on the antibacterial activity of green synthesized silver nanoparticles. Microb. Pathog. 102, 133–142.
Ahmad, T., Wani, I.A., Manzoor, N., Ahmed, J., Asiri, A.M., 2013. Biosynthesis, structural characterization and antimicrobial activity of gold and silver nanoparticles. Colloids Surfaces B Biointerfaces 107, 227–234.
Ahmed, S., Ahmad, M., Swami, B.L., Ikram, S., 2016. A review on plants extract mediated synthesis of silver nanoparticles for antimicrobial applications: a green expertise. J. Adv. Res. 7, 17–28.
Amooaghaie, R., Saeri, M.R., Azizi, M., 2015. Synthesis, characterization and biocompatibility of silver nanoparticles synthesized from Nigella sativa leaf extract in comparison with chemical silver nanoparticles. Ecotoxicol. Environ. Saf. 120, 400–408.
Araújo, J.N., Tofanello, A., da Silva, V.M., Sato, J.A.P., Squina, F.M., Nantes, I.L., Garcia, W., 2017. Photobiosynthesis of stable and functional silver/silver chloride nanoparticles with hydrolytic activity using hyperthermophilic β-glucosidases with industrial potential. Int. J. Biol. Macromol. 102, 84–91.
Ashraf, J.M., Ansari, M.A., Khan, H.M., Alzohairy, M.A., Choi, I., 2016. Green synthesis of silver nanoparticles and characterization of their inhibitory effects on AGEs formation using biophysical techniques. Sci. Rep. 6, 20414.
Davoodbasha, M., Kim, S.-C., Lee, S.-Y., Kim, J.-W., 2016. The facile synthesis of chitosan-based silver nano-biocomposites via a solution plasma process and their potential antimicrobial efficacy. Arch. Biochem. Biophys. 605, 49–58.
El-Naggar, N.E.-A., Hussein, M.H., El-Sawah, A.A., 2017. Bio-fabrication of silver nanoparticles by phycocyanin, characterization, in vitro anticancer activity against breast cancer cell line and in vivo cytotxicity. Sci. Rep. 7, 10844.
Gopinath, V., MubarakAli, D., Priyadarshini, S., Priyadharsshini, N.M., Thajuddin, N., Velusamy, P., 2012. Biosynthesis of silver nanoparticles from Tribulus terrestris and its antimicrobial activity: a novel biological approach. Colloids Surfaces B Biointerfaces 96, 69–74.
Gopinath, V., Priyadarshini, S., Al-Maleki, A., Alagiri, M., Yahya, R., Saravanan, S., Vadivelu, J., 2016. In vitro toxicity, apoptosis and antimicrobial effects of phyto-mediated copper oxide nanoparticles. RSC Adv. 6, 110986–110995.
Gopinath, V., Priyadarshini, S., Loke, M.F., Arunkumar, J., Marsili, E., MubarakAli, D., Velusamy, P., Vadivelu, J., 2017. Biogenic synthesis, characterization of antibacterial silver nanoparticles and its cell cytotoxicity. Arabian J. Chem. 10, 1107–1117.
Gopinath, V., Priyadarshini, S., Meera Priyadharsshini, N., Pandian, K., Velusamy, P., 2013. Biogenic synthesis of antibacterial silver chloride nanoparticles using leaf extracts of Cissus quadrangularis Linn. Mater. Lett. 91, 224–227.
Gopinath, V., Priyadarshini, S., MubarakAli, D., Loke, M.F., Thajuddin, N., Alharbi, N.S., Yadavalli, T., Alagiri, M., Vadivelu, J., 2019. Anti-Helicobacter pylori, cytotoxicity

and catalytic activity of biosynthesized gold nanoparticles: multifaceted application. Arabian J. Chem. 12, 33–40.
Gopinath, V., Priyadarshini, S., Venkatkumar, G., Saravanan, M., Mubarak Ali, D., 2015. *Tribulus terrestris* leaf mediated biosynthesis of stable antibacterial silver nanoparticles. Pharm. Nanotechnol. 3, 26–34.
Gopinath, V., Velusamy, P., 2013. Extracellular biosynthesis of silver nanoparticles using Bacillus sp. GP-23 and evaluation of their antifungal activity towards Fusarium oxysporum. Spectrochim. Acta Mol. Biomol. Spectrosc. 106, 170–174.
Hu, W., Chen, S., Li, X., Shi, S., Shen, W., Zhang, X., Wang, H., 2009. In situ synthesis of silver chloride nanoparticles into bacterial cellulose membranes. Mater. Sci. Eng. C 29, 1216–1219.
Hulkoti, N.I., Taranath, T.C., 2014. Biosynthesis of nanoparticles using microbes—a review. Colloids Surfaces B Biointerfaces 121, 474–483.
Iniyan, A.M., Kannan, R.R., Joseph, F.-J.R.S., Mary, T.R.J., Rajasekar, M., Sumy, P.C., Rabel, A.M., Ramachandran, D., Vincent, S.G.P., 2017. In vivo safety evaluation of antibacterial silver chloride nanoparticles from Streptomyces exfoliatus ICN25 in zebrafish embryos. Microb. Pathog. 112, 76–82.
Jha, A.K., Prasad, K., Kumar, V., Prasad, K., 2009. Biosynthesis of silver nanoparticles using eclipta leaf. Biotechnol. Prog. 25, 1476–1479.
Judith Vijaya, J., Jayaprakash, N., Kombaiah, K., Kaviyarasu, K., John Kennedy, L., Jothi Ramalingam, R., Al-Lohedan, H.A., V.M, M.-A., Maaza, M., 2017. Bioreduction potentials of dried root of Zingiber officinale for a simple green synthesis of silver nanoparticles: antibacterial studies. J. Photochem. Photobiol. B Biol. 177, 62–68.
Lee, C.-K., Fang, J.-M., Cheng, Y.-S., 1995. Norditerpenes from *Juniperus chinensis*. Phytochemistry 39, 391–394.
Ma, J., Lü, X., Huang, Y., 2011. Genomic analysis of cytotoxicity response to nanosilver in human dermal fibroblasts. J. Biomed. Nanotechnol. 7, 263–275.
Maruthupandy, M., Rajivgandhi, G., Muneeswaran, T., Song, J.-M., Manoharan, N., 2018. Biologically synthesized zinc oxide nanoparticles as nanoantibiotics against ESBLs producing gram negative bacteria. Microb. Pathog. 121, 224–231.
MubarakAli, D., Thajuddin, N., Jeganathan, K., Gunasekaran, M., 2011. Plant extract mediated synthesis of silver and gold nanoparticles and its antibacterial activity against clinically isolated pathogens. Colloids Surfaces B Biointerfaces 85, 360–365.
Naik, R.R., Stringer, S.J., Agarwal, G., Jones, S.E., Stone, M.O., 2002. Biomimetic synthesis and patterning of silver nanoparticles. Nat. Mater. 1, 169–172.
Nordin, N., Salama, S.M., Golbabapour, S., Hajrezaie, M., Hassandarvish, P., Kamalidehghan, B., Majid, N.A., Hashim, N.M., Omar, H., Fadaienasab, M., 2014. Anti-ulcerogenic effect of methanolic extracts from Enicosanthellum pulchrum (King) Heusden against ethanol-induced acute gastric lesion in animal models. PLoS One 9 e111925.
Orhan, N., Orhan, I.E., Ergun, F., 2011. Insights into cholinesterase inhibitory and antioxidant activities of five Juniperus species. Food Chem. Toxicol. 49, 2305–2312.
Rajabnia, T., Meshkini, A., 2018. Fabrication of adenosine 5′-triphosphate-capped silver nanoparticles: enhanced cytotoxicity efficacy and targeting effect against tumor cells. Process Biochem. 65, 186–196.
Rasheed, T., Bilal, M., Iqbal, H.M.N., Li, C., 2017. Green biosynthesis of silver nanoparticles using leaves extract of Artemisia vulgaris and their potential biomedical applications. Colloids Surfaces B Biointerfaces 158, 408–415.
Rizwan, M., Yahya, R., Hassan, A., Yar, M., Anita Omar, R., Azari, P., Danial Azzahari, A., Selvanathan, V., Rageh Al-Maleki, A., Venkatraman, G., 2018. Synthesis of a novel organosoluble, biocompatible, and antibacterial chitosan derivative for biomedical applications. J. Appl. Polym. Sci. 135.
Saravanakumar, K., Chelliah, R., Shanmugam, S., Varukattu, N.B., Oh, D.-H., Kathiresan, K., Wang, M.-H., 2018. Green synthesis and characterization of biologically active nanosilver from seed extract of Gardenia jasminoides Ellis. J. Photochem. Photobiol. B Biol. 185, 126–135.
Saravanan, M., Gopinath, V., Chaurasia, M.K., Syed, A., Ameen, F., Purushothaman, N., 2018. Green synthesis of anisotropic zinc oxide nanoparticles with antibacterial and cytofriendly properties. Microb. Pathog. 115, 57–63.
Singh, M., Sahareen, T., 2017. Investigation of cellulosic packets impregnated with silver nanoparticles for enhancing shelf-life of vegetables. LWT - Food Sci. Technol. (Lebensmittel-Wissenschaft -Technol.) 86, 116–122.
Suresh, A.K., Pelletier, D.A., Wang, W., Moon, J.-W., Gu, B., Mortensen, N.P., Allison, D.P., Joy, D.C., Phelps, T.J., Doktycz, M.J., 2010. Silver nanocrystallites: biofabrication using shewanella oneidensis, and an evaluation of their comparative toxicity on gram-negative and gram-positive bacteria. Environ. Sci. Technol. 44, 5210–5215.
Taha, H., Arya, A., Paydar, M., Looi, C.Y., Wong, W.F., Murthy, C.R.V., Noordin, M.I., Ali, H.M., Mustafa, A.M., Hadi, A.H.A., 2014. Upregulation of insulin secretion and downregulation of pro-inflammatory cytokines, oxidative stress and hyperglycemia in STZ-nicotinamide-induced type 2 diabetic rats by Pseuduvaria monticola bark extract. Food Chem. Toxicol. 66, 295–306.
Wang, Y., Qiao, Y., Wang, P., Li, Q., Xia, C., Ju, M., 2018. Bio fabrication of silver nanoparticles as an effective wound healing agent in the wound care after anorectal surgery. J. Photochem. Photobiol. B Biol. 178, 457–462.
Xie, T., Liao, Z., Lei, H., Fang, X., Wang, J., Zhong, Q., 2017. Antibacterial activity of food-grade chitosan against Vibrio parahaemolyticus biofilms. Microb. Pathog. 110, 291–297.
Zayed, M.F., Eisa, W.H., El-kousy, S.M., Mleha, W.K., Kamal, N., 2019. Ficus Retusa-Stabilized Gold and Silver Nanoparticles: Controlled Synthesis, Spectroscopic Characterization, and Sensing Properties. Spectrochimica Acta Part A: Molecular and Biomolecular Spectroscopy.